Cerebral Cortex Advance Access published November 10, 2011

Cerebral Cortex
doi:10.1093/cercor/bhr319

Theta Phase Modulates Multiple Layer-Specific Oscillations in the CA1 Region

Robson Scheffer-Teixeira[1,2], Hindiael Belchior[1,2], Fábio V. Caixeta[1,2], Bryan C. Souza[1,2], Sidarta Ribeiro[1] and Adriano B. L. Tort[1]

[1]Brain Institute, Federal University of Rio Grande do Norte, Natal, Rio Grande do Norte 59056, Brazil and [2]Edmond and Lily Safra International Institute of Neuroscience of Natal, Natal, Rio Grande do Norte 59066, Brazil

Address correspondence to Adriano B. L. Tort, Brain Institute, Federal University of Rio Grande do Norte, Rua Nascimento de Castro, 2155-Lagoa Nova, Natal, Rio Grande do Norte 59056-450, Brazil. Email: tort@neuro.ufrn.br.

It was recently proposed that fast gamma oscillations (60–150 Hz) convey spatial information from the medial entorhinal cortex (EC) to the CA1 region of the hippocampus. However, here we describe 2 functionally distinct oscillations within this frequency range, both coupled to the theta rhythm during active exploration and rapid eye movement sleep: an oscillation with peak activity at ~80 Hz and a faster oscillation centered at ~140 Hz. The 2 oscillations are differentially modulated by the phase of theta depending on the CA1 layer; theta-80 Hz coupling is strongest at stratum lacunosum–moleculare, while theta-140 Hz coupling is strongest at stratum oriens–alveus. This laminar profile suggests that the ~80 Hz oscillation originates from EC inputs to deeper CA1 layers, while the ~140 Hz oscillation reflects CA1 activity in superficial layers. We further show that the ~140 Hz oscillation differs from sharp wave–associated ripple oscillations in several key characteristics. Our results demonstrate the existence of novel theta–associated high-frequency oscillations and suggest a redefinition of fast gamma oscillations.

Keywords: amplitude modulation, cross-frequency coupling, gamma, hippocampal oscillations, local field potential

Introduction

The frequency of gamma oscillations was recently suggested to route the information flow into CA1: according to this hypothesis, slow gamma (20–50 Hz) conveys information arriving from CA3, whereas fast gamma (60–150 Hz) signals entorhinal cortex (EC) inputs (Colgin et al. 2009). However, by studying the patterns of cross-frequency coupling (CFC) in CA1, we show here that this fast gamma range comprises at least 2 distinct oscillatory activities.

Brain oscillations of different frequencies can interact in several ways (Jensen and Colgin 2007; Canolty and Knight 2010). Phase–amplitude coupling, or nesting, is a particular type of CFC defined as the amplitude modulation of a higher frequency oscillation by the phase of a slower rhythm (Kramer et al. 2008; Canolty and Knight 2010; Tort et al. 2010; Onslow et al. 2011). Phase–amplitude coupling occurs in various brain regions and species such as rodents (Bragin et al. 1995; Buzsaki et al. 2003; Wulff et al. 2009), sheep (Kendrick et al. 2011), monkeys (Lakatos et al. 2005; Whittingstall and Logothetis 2009), and humans (Vanhatalo et al. 2004; Miller et al. 2010; Voytek et al. 2010). Recent evidence suggests that phase–amplitude coupling is involved in working memory and decision making (Canolty et al. 2006; Tort et al. 2008; Axmacher et al. 2010), attentional selection (Schroeder and Lakatos 2009), and reward signaling (Cohen et al. 2009). In the hippocampus, theta (5–10 Hz) phase modulates gamma amplitude (Stumpf 1965; Soltesz and Deschenes 1993; Bragin et al. 1995; Buzsaki et al. 2003), an oscillatory coupling that has been hypothesized to underlie learning and memory retrieval (Lisman and Idiart 1995; Tort et al. 2009). In spite of recent progress, little is known about general CFC characteristics in the hippocampus and other brain regions.

In the present work, we characterized the patterns of phase–amplitude CFC in CA1 during theta-associated states. We found that theta phase modulates 2 nonoverlapping higher frequency oscillations, which we refer to as high gamma (HG, 60–100 Hz, peak activity ~80 Hz) and high-frequency oscillations (HFOs, 120–160 Hz, peak activity ~140 Hz). The patterns of theta-phase coupling are layer-specific and indicate that HG oscillations reflect EC inputs to deep CA1 layers, while HFOs likely result from local CA1 activity in superficial layers. These findings demonstrate a novel form of fast network oscillations at ~140 Hz that co-occur with theta waves but differ from fast gamma oscillations. We further show that theta-associated HFOs also differ from sharp wave–associated ripple oscillations.

Materials and Methods

Surgery

All animal work including housing, surgical, and recording procedures were in strict accordance with the National Institutes of Health guidelines and were approved by the Edmond and Lily Safra International Institute of Neuroscience of Natal Committee for Ethics in Animal Experimentation (permit # 03/2010). We used male Wistar and Long–Evans rats (2–3 months age, 250–350 g) from our breeding colony, kept under a 12-h light–dark cycle (lights on at 07:00). Eight Wistar rats were anesthetized with ketamine and xylazine and implanted with 4 × 8 multielectrode arrays (50 μm Teflon-coated tungsten microwires; electrode spacing: 300 μm; impedance: ~1 MΩ at 1 kHz) targeting the left hippocampal CA1 region (centered at anteroposterior (AP): −3.6 mm and mediolateral (ML): −1.6 mm from Bregma; and dorsoventral (DV): −2.4 mm from the pial surface). Six additional animals (3 Wistar and 3 Long–Evans rats) were implanted with electrode bundles consisting of 6–8 staggered wires, which were aligned and equally spaced (250 μm) in the vertical axis. The tip of the bundle was placed in the upper blade of the dentate gyrus (AP: −3.6 mm, ML: −2.5 mm, DV: −2.9 mm). The position of the electrodes along the bundle was estimated by responses evoked by perforant path stimulation (single pulse, 500 μA) along with other standard electrophysiological parameters such as presence of ripple oscillations and multiunit activity at the pyramidal cell layer, theta phase reversal across stratum radiatum (Brankack et al. 1993), and maximal theta power at the hippocampal fissure (Bragin et al. 1995).

Electrophysiological Recordings

Experiments began 7–14 days after surgery and consisted of electrophysiological and video recordings of freely moving animals in a rectangular chamber (50 × 35 × 35 cm) placed in a dimly lighted room. Recordings were carried out in the afternoon across the spontaneous sleep–wake cycle. Continuous electrophysiological recordings were performed for up to 3 h using a multichannel

© The Author 2011. Published by Oxford University Press. All rights reserved.
For permissions, please e-mail: journals.permissions@oup.com

Downloaded from http://cercor.oxfordjournals.org/ at Brigham & Women's Hospital on November 29, 2012

acquisition processor (MAP; Plexon Inc, Dallas, TX). Local field potentials (LFPs) were preamplified (1000×), filtered (0.7–300 Hz), and digitized at 1000 Hz. Plexon HST/32V-G20 high-impedance headstages and PBX preamplifier models were used. The animals were video recorded throughout the sessions. The placement of electrodes in CA1 was confirmed by inspecting coronal brain sections stained with cresyl violet.

Data Analysis

All analyses were performed using built-in and custom written routines in MATLAB (MathWorks, Natick, MA).

Estimation of Phase–Amplitude Coupling

To assess phase–amplitude coupling, we used the modulation index (MI) and associated comodulation analysis first introduced in Tort et al. (2008) and later described in detail in Tort et al. (2010). The MI measures CFC strength between 2 frequency ranges of interest: a phase-modulating (f_p) and an amplitude-modulated (f_A) frequency. Briefly, the MI is obtained as follows: the phases of f_p are binned into eighteen 20° intervals and the mean amplitude of f_A associated to each phase bin is computed; the mean amplitude is subsequently normalized by dividing each bin value by the sum over all bins, creating a phase–amplitude distribution-like function (see Supplementary Fig. S1). A uniform phase–amplitude distribution means that the f_A amplitude is on average the same for all f_p phase bins, which happens in the absence of phase–amplitude coupling. The higher the coupling, the further away the phase–amplitude distribution gets from the uniform distribution. The difference between the empirical phase–amplitude distribution (P) and the uniform distribution (U) can be assessed by the Kullback–Leibler divergence: $KL(P,U) = \log(N_{bins}) + \sum p_j \log(p_j)$, where $N_{bins} = 18$ is the number of phase bins and p_j is the "amplitude probability" of the j-th phase bin. Finally, the MI is given by $KL(P,U)/\log(N_{bins})$, which is a measure bounded between 0 and 1.

To obtain the comodulation map, the MI is computed for several frequency band pairs (f_p, f_A) and the MI values are expressed in a bidimensional pseudocolor plot (see Supplementary Fig. S1). The frequency bands are narrow-filtered signals (phase frequencies: 4-Hz bandwidths; amplitude frequencies: 10-Hz bandwidths), and each coordinate in the comodulogram represents the center frequency. The x- and y-axis denote the frequency bands analyzed as phase-modulating (f_p) and amplitude-modulated (f_A), respectively. Therefore, warm colors in a given (f_p, f_A) coordinate means that the phase of f_p modulates the amplitude of f_A (Supplementary Fig. S1).

Each comodulation map shown in this work was computed from a single LFP time series exhibiting prominent theta activity. We used continuous time series for theta oscillations associated with the active waking state and concatenated data for rapid eye movement (REM) sleep theta. In this latter case, the LFP signals were filtered before concatenation to avoid edge effects; that is, for each pair of frequencies (f_p, f_A), we first computed the instantaneous phase and amplitude time series of the entire LFP trace and then used the segments with high theta power associated with REM sleep for the comodulation analysis. The total length of the time series used to compute the comodulation maps varied from 60 to 300 s and is indicated in the figure legends.

The time–frequency amplitude distribution time locked to the theta peak shown in Figure 3*C* and Supplementary Figure S5 was obtained by first localizing the time points corresponding to the theta peaks and then computing the mean amplitude envelope centered at these time points; this procedure was performed for several narrow-filtered frequency bands of 4-Hz bandwidth, covering 10–200 Hz with 2-Hz steps. For better comparison across frequencies, the amplitudes were z-scored to correct for $1/f$. The trace at the bottom panel shows the average raw signal also triggered by the same theta peaks.

The time course of CFC strength shown in the third and fourth panels of Figure 2*A* was obtained by computing the MI value for wideband filtered signals in the HFO, HG, and theta bands, using 60-s moving windows with 40-s overlap. In Supplementary Figure S3, we repeated this analysis using 30-, 15-, and 6-s time windows with 15-, 10-, and 4-s overlap, respectively. Except for Figure 2 and Supplementary Figure S3, only periods of high theta power were used to assess CFC.

Filter Settings and Amplitude and Phase Time Series Extraction

Filtering was obtained using a linear finite impulse response filter by means of the "eegfilt" function from the EEGLAB Toolbox (Delorme and Makeig 2004). The filter order depends on the low-frequency cutoff, and it is given by 3 times the ratio of the sampling frequency to the low-frequency cutoff (rounded to the nearest integer toward zero). The eegfilt function calls the MATLAB "filtfilt" function, which applies the filter forward and then again backwards to ensure that phase delays introduced by the filter are nullified. The filter employed is a least square linear-phase FIR filter, which is designed using the MATLAB "firls" function.

The instantaneous amplitude and the phase time series of a filtered signal were computed from the Hilbert transform, which was obtained by the "hilbert" function from the Signal Processing Toolbox.

Spectral Analyses

Power spectra estimation was done by means of the Welch periodogram method using the "pwelch" function from the Signal Processing Toolbox (50% overlapping Hamming windows with a length of 4 s). The high-frequency power spectra for individual electrodes shown in Figure 4*B* inset was smoothed using a 5-Hz moving average (no smoothing was applied in Fig. 2*B* and in the group result shown in Fig. 4*D*). Time–frequency spectral decompositions were obtained by using the "spectrogram" function from the Signal Processing Toolbox. The result shown in Figure 2*A* used 20-s time windows with 10-s overlap, and the plot in Supplementary Figure S4C used 4-s windows with 2-s overlap. The cross-correlation shown in Figure 3*D* was obtained using the "xcorr" function (with the "coeff" option) from the Signal Processing Toolbox. We note that since we calculated the cross-correlation between amplitude envelopes, which are positive-valued functions, the cross-correlation values are always positive, even at large lags.

The time course of theta power shown in the second panel of Figure 2*A* was obtained by integrating the power values in the theta band in 60-s moving windows with 40-s overlap (i.e., the same sliding windows as in the CFC analyses depicted in the third and fourth panels of Fig. 2*A*). In Supplementary Figure S3, we show equivalent results using shorter time windows.

Estimation of REM Sleep and Active Waking Periods

We used a previously described quantitative spectral algorithm for behavioral state classification based on the analysis of LFPs (Gervasoni et al. 2004; Dzirasa et al. 2006). Briefly, a 2-dimensional state space is defined by 2 spectral amplitude ratios calculated by dividing integrated spectral amplitudes at selected frequency bands, which include power at delta, theta, and gamma bands. A scatter plot of the amplitude ratios (state space) reveals distinct clusters that correspond to different sleep–wake states (see Gervasoni et al. 2004). The classification provided by the state-space approach was further confirmed by the visual inspection of video recordings.

Results

Theta Phase Modulates Multiple Higher Frequency Oscillations in CA1

To characterize phase–amplitude CFC in CA1 during spontaneous theta–associated behaviors, we first used multielectrode arrays to record LFPs across the sleep–wake cycle from 8 rats (Fig. 1*A*,*B*). During both active waking and REM sleep, we found very prominent coupling between theta and higher frequency oscillations in all animals. More specifically, LFPs were subjected to comodulation analysis (Tort et al. 2010), which shows the level of phase–amplitude coupling between several frequency pairs in a single bidimensional map (warm colors in an (x, y) entry indicates that the phase of x modulates the amplitude of y; see Supplementary Fig. S1). The comodulation maps revealed the existence of coupling between the

Downloaded from http://cercor.oxfordjournals.org/ at Brigham & Women's Hospital on November 29, 2012

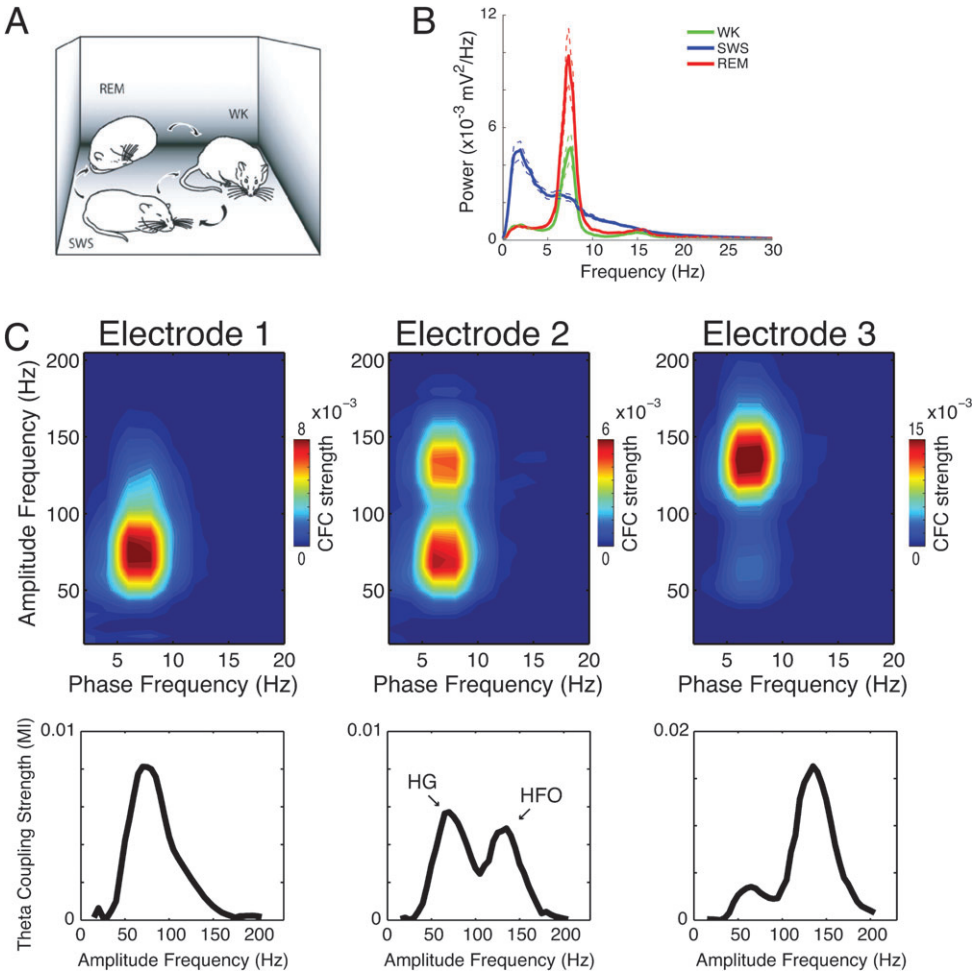

Figure 1. Theta phase modulates multiple higher frequency oscillations. (*A*) Sleep–wake cycle in freely moving rats was monitored in a familiar arena (adapted from Ribeiro et al. 2007). (*B*) Representative power spectra of 3 behavioral states (mean ± standard error of the mean over all electrodes in an array). WK—active waking; SWS—slow-wave sleep. (*C*) Top: Comodulation maps obtained during REM sleep (180 s analyzed) from 3 simultaneously recorded electrodes. Warm colors indicate that the *x*-phase modulates *y*-amplitude (see Supplementary Fig. S1). Bottom: Theta coupling strength as a function of modulated frequency (mean over all comodulogram entries in the theta range).

theta phase and the amplitude of 2 circumscribed, non-overlapping rhythms: HG and HFOs (Fig. 1*C*). A striking finding was that while some electrodes exhibited much higher theta phase modulation of HG than HFOs, the exact opposite was observed in other simultaneously recorded electrodes (Fig. 1*C*, left and right panels). There were also cases of electrodes presenting a mixed CFC pattern, in which both HG and HFOs were modulated by theta phase at roughly equal strength (Fig. 1*C*, middle panel). Of note, we did not find prominent modulation of low gamma (LG, 30–60 Hz) activity by theta phase (see Discussion). Importantly, CFC patterns within electrodes were stable across days (Supplementary Fig. S2).

Theta Phase Modulation of HG and HFO Amplitude is Highly Dependent on Theta Power

Next, we searched for possible dependencies of theta-HG and theta-HFO coupling on theta power level. In Figure 2*A*, we show the time course of theta power levels across the sleep–wake cycle in 2 simultaneously recorded electrodes in a multielectrode array (Electrodes 4 and 5, second panel from top; the top panel shows the time–frequency power spectrum of Electrode 5). While one electrode (Electrode 4) exhibited prominent theta-HFO coupling ("HFO electrode"), the other (Electrode 5) had prominent theta-HG coupling ("HG electrode"; see Fig. 2*D*). The power spectral density (PSD) of the LFP signal recorded from the HFO electrode during the period depicted in Figure 2*A* exhibited a power peak in the HFO band, which was not apparent in the HG electrode (Fig. 2*B*).

As expected (Vanderwolf 1969; Timo-Iaria et al. 1970), the power of theta oscillations varied considerably during each recording session, mainly on account of the animal's behavior across the sleep–wake cycle. Theta power variations were qualitatively similar in all electrodes, and, as shown in Figure 2*A* (bottom 2 panels), the intensity of theta-HG and theta-HFO coupling followed very closely the time course of theta power. In fact, linear correlation analysis showed that CFC intensity positively correlated with theta power (Fig. 2*C*; see also Supplementary Fig. S3). Qualitatively similar results were found in all other animals (not shown). Thus, the higher the theta power, the higher the theta-HG and theta-HFO coupling intensity.

HFOs and HG Occur at Different Theta Phases

The results above indicate that the modulation of HFOs and HG by theta phase is coincident on a time scale of seconds to minutes, that is, during the periods of high theta activity. Next,

Downloaded from http://cercor.oxfordjournals.org/ at Brigham & Women's Hospital on November 29, 2012

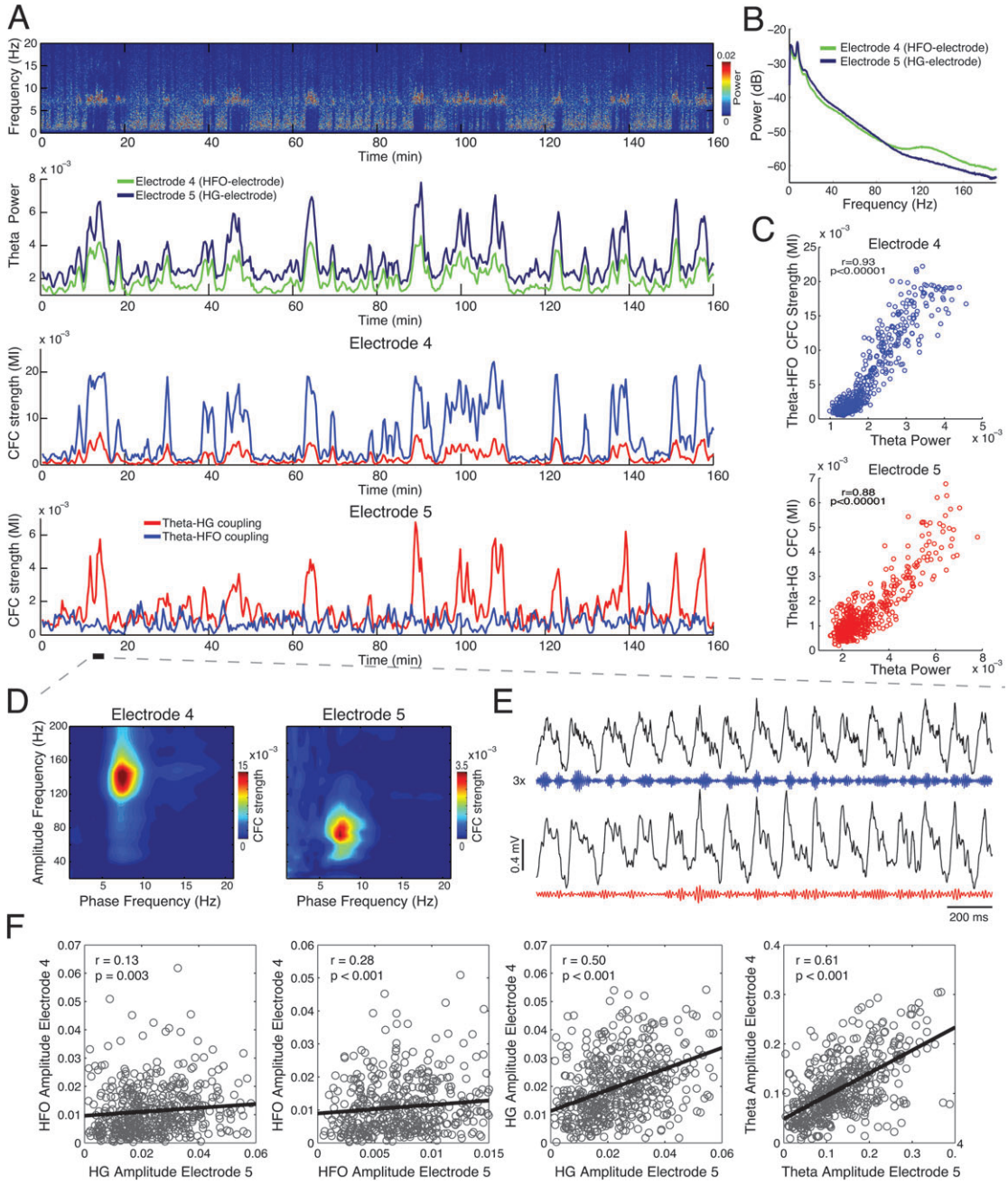

Figure 2. Theta-HG and theta-HFO coupling levels are positively correlated with theta power. (*A*) Top panel: Time–frequency power spectrum showing periods of theta activity alternating with periods of delta activity (Electrode 5). Window length: 20 s; overlap: 10 s. Second panel: Time course of mean theta power in 2 simultaneously recorded electrodes. Bottom 2 panels: Theta-HG (red) and theta-HFO (blue) CFC strength for the same 2 electrodes, as labeled. MI = modulation index (see Materials and Methods). Sliding time windows of 60 s with 40-s overlap were used in the bottom 3 panels (for the same analysis using shorter time windows, see Supplementary Fig. S3). (*B*) Power spectra computed for the whole period depicted in *A* showing a peak in the HFO band for Electrode 4. (*C*) Scatter plots of CFC strength versus theta power. (*D*) Comodulation maps computed for a 60-s period of high theta activity (indicated by the horizontal black bar in *A*). (*E*) LFPs (black), HFO- (blue), and HG-filtered (red) signals obtained during the same epoch as in *D* (only 2 s are shown; top and bottom traces are from Electrodes 4 and 5, respectively). Notice high theta coherence between electrodes and low coherence in the amplitude variations of HFOs and HG. (*F*) Scatter plots of the amplitude of the oscillations recorded from Electrode 4 versus Electrode 5, for multiple rhythms (as labeled). Notice that the amplitudes of HFOs and HG are not strongly correlated (see also Supplementary Fig. S4).

we investigated HG and HFO activity on a finer temporal scale, such as that of a theta cycle. In Figure 2*E*, we show the raw LFP and HG- and HFO-filtered signals obtained from the same HG and HFO electrodes as above during a 2-s snippet of high theta power. While the amplitude of theta oscillations varied in a similar way in both electrodes, the instantaneous amplitudes of HG and HFOs were not as strongly correlated (Fig. 2*F*). On a group level, during periods of high theta activity, the zero-lag correlation between HG and HFO amplitudes was weak in all animals studied (4 examples are shown in Supplementary Fig. S4A), even for electrodes exhibiting a mixed CFC pattern (Supplementary Fig. S4B).

Visual inspection of filtered signals, however, suggested that HFO and HG amplitude variations could be correlated with a time lag. Figure 3*A* shows a theta cycle simultaneously recorded from another pair of HG and HFO electrodes in

Downloaded from http://cercor.oxfordjournals.org/ at Brigham & Women's Hospital on November 29, 2012

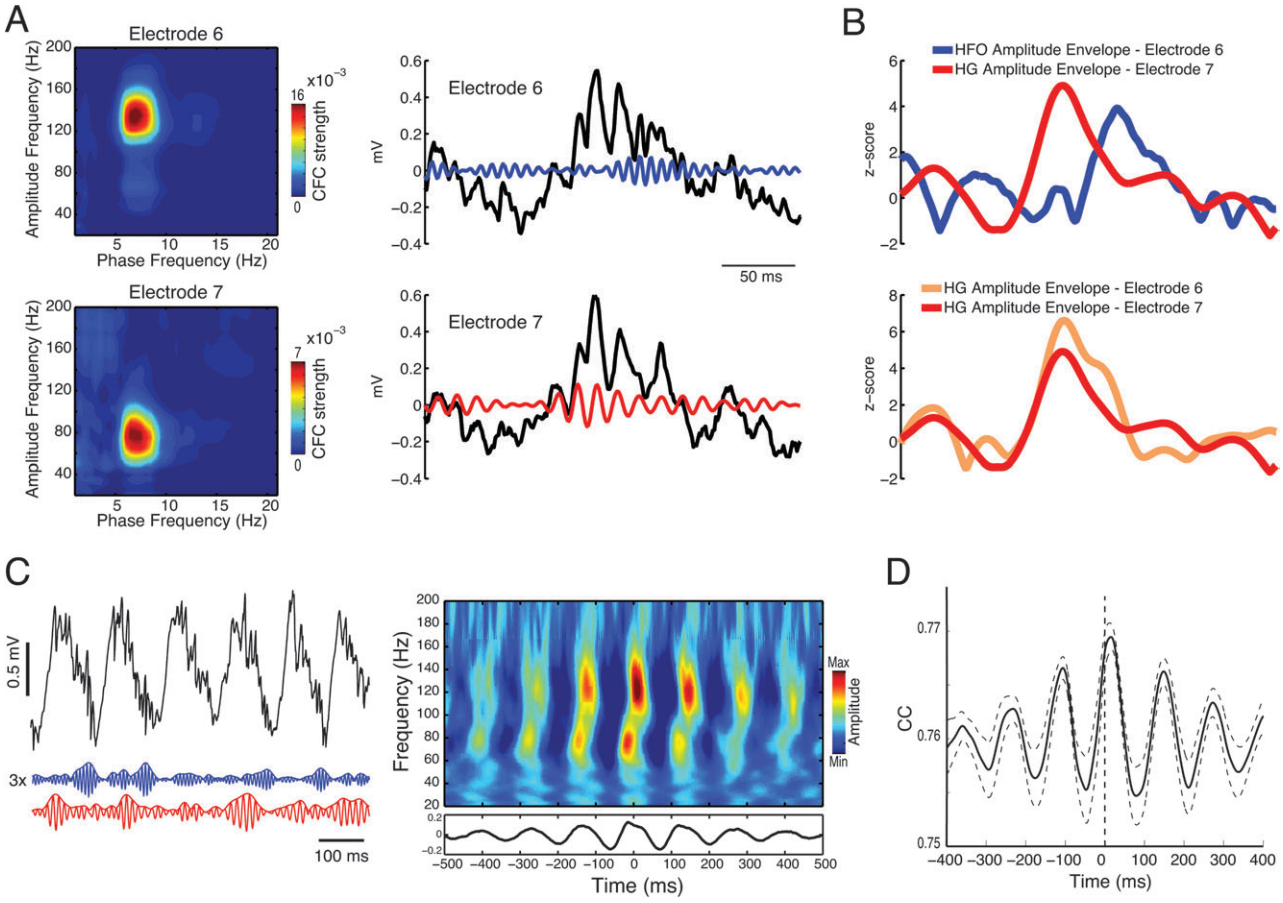

Figure 3. HG and HFO amplitudes peak at different theta phases. (*A*) Comodulation maps obtained during active waking (120 s analyzed) for an HFO and an HG electrode (left panels) and simultaneously recorded LFPs (right panels). The associated HFO- (blue) and HG-filtered (red) signals are also shown. Notice that peak HG activity precedes peak HFO activity within the theta cycle. (*B*) Top traces: Amplitude envelopes of the HFO- and HG-filtered signals shown in *A*, highlighting different temporal dynamics. Bottom traces: Amplitude envelopes of HG-filtered signals from Electrodes 6 and 7, as labeled (same trace as above for Electrode 7). Notice similar HG dynamics in both electrodes. (*C*) Left: LFP (black), HFO- (blue), and HG-filtered (red) signals (and amplitude envelopes) from an electrode presenting mixed CFC pattern. Right: Time–frequency amplitude distribution time locked to the theta peak showing maximal HG and HFO activity at different theta phases (see also Supplementary Fig. S5). (*D*) Mean cross-correlation (CC) between the amplitude envelopes of HG (reference signal) and HFOs during periods of high theta activity. The HG- and HFO-filtered signals were obtained from electrodes with prominent theta-HG and theta-HFO coupling, respectively. Dashed lines correspond to ± standard error of the mean.

a multielectrode array. Note that while the HG oscillation can be observed in both electrodes, HFOs are most apparent in the HFO electrode (Fig. 3*A*, right panels). Importantly, note in this example that HG and HFOs have different time courses of amplitude variations within the theta cycle (Fig. 3*B* top panel). HG and HFO peak activity also tended to occur in different theta phases in electrodes presenting a mix CFC pattern (Fig. 3*C*; see also Supplementary Figs S5 and S6). On a group level, we found that the HG peak activity preceded HFO peak activity by ~16 ms (Fig. 3*D*).

Different Patterns of Phase–Amplitude Coupling Across CA1 Layers

Histological sections confirmed the location of the multielectrode arrays in CA1; given the curved geometry of the hippocampus, different electrodes in the rectangular array necessarily ended at different distances from the pyramidal cell layer, either below or above (see Supplementary Fig. S7). We next sought to determine whether this could underlie interelectrode differences observed in CFC patterns.

In Figure 4*A*, we show another representative pair of HG (bottom) and HFO (top) electrodes simultaneously recorded in a multielectrode array. Notice that the amplitude of theta oscillations is higher in the HG electrode (see also Fig. 4*B*). On a group level, the mean power spectrum over all HG and HFO electrodes within animals revealed higher theta power in HG electrodes (4 examples are shown in Fig. 4*C*). Since theta power is well known to vary across CA1 layers, from a minimum in stratum oriens–alveus to a maximum near the hippocampal fissure (Bragin et al. 1995; Lubenov and Siapas 2009), this result suggests that theta-HG coupling is stronger in deeper CA1 layers (where theta amplitude is higher), whereas theta-HFO coupling occurs in more superficial CA1 layers (where theta amplitude is lower). Importantly, putative superficial electrodes presenting lower levels of theta power and strong theta-HFO coupling also exhibited a clear power peak in the HFO band during periods of high theta activity (Fig. 4*B*,*D*).

To further investigate this hypothesis (we considered the reconstruction of the precise location of the 32 electrode tips in the 4 × 8 array not reliable), we carried out a new set of experiments using bundles of electrodes of different lengths, specifically designed to target different CA1 depths ($n = 6$ rats). This allowed us to directly assess the topological dependence of CFC on CA1 layer. As suggested by the multielectrode array

Downloaded from http://cercor.oxfordjournals.org/ at Brigham & Women's Hospital on November 29, 2012

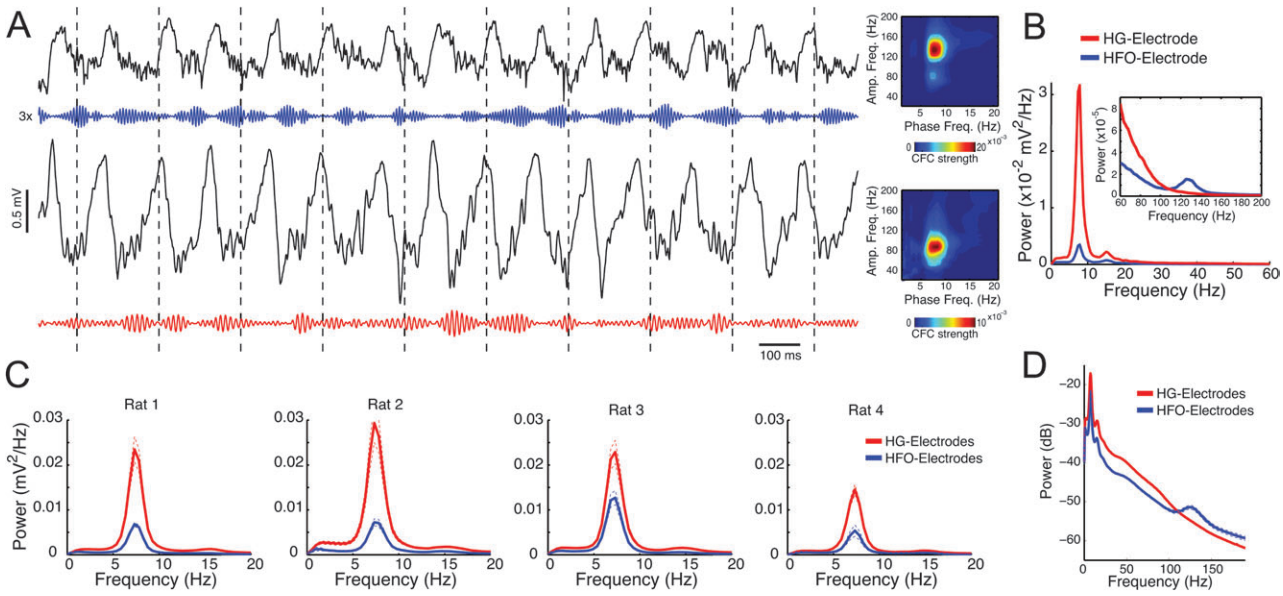

Figure 4. HG electrodes have higher theta power than HFO electrodes. (*A*,*B*) LFPs (black), HFO- (blue) and HG-filtered (red) signals from an HFO (top) and an HG electrode (bottom) recorded simultaneously during 100 s of active exploration (*A*), and their power spectra (*B*). (*C*) Mean power spectra over HFO and HG electrodes in 4 representative animals. (*D*) Group power spectra (mean over all animals). Only active waking and REM sleep periods were used to compute the power spectra in *C* and *D*.

recordings, theta-HFO coupling was prominent at superficial CA1 layers (stratum oriens–alveus), while theta-HG coupling was most prominent closer to stratum lacunosum–moleculare (Fig. 5*A*,*B*; see also Supplementary Figs S5 and S6). The switch between theta-HFO and theta-HG coupling occurred at the pyramidal cell layer: electrodes at stratum pyramidale exhibiting characteristic ripple oscillations (Fig. 5*A* and Supplementary Fig. S6) and multiunit activity (Supplementary Fig. S6) exhibited mainly theta-HG coupling; electrodes in stratum oriens–alveus near the pyramidal layer exhibited mixed CFC patterns, whereas more superficial electrodes exhibited mainly theta-HFO coupling (Fig. 5 and Supplementary Fig. S6). Of note, these experiments also revealed that theta phase modulates a wideband of very high frequencies in dentate gyrus, which were not as circumscribed as the HFOs seen in stratum oriens–alveus (Fig. 5*A*).

Lastly, using the pyramidal layer theta as the reference signal, we found that maximal multiunit activity occurred near the trough of the theta cycle, while the maximal amplitude of HG and HFO occurred near the peak and at the descending phase of the theta cycle, respectively (Fig. 6).

Discussion

We have shown that theta phase modulates the amplitude of 2 nonoverlapping higher frequency oscillations in CA1. A striking finding was that, in simultaneous multisite recordings of field potentials, some electrodes exhibited prominent theta modulation of HG, while in other electrodes theta modulated HFOs instead (Fig. 1). Since CFC patterns within electrodes were stable (Supplementary Fig. S2), we reasoned that hardwired anatomical variables should account for interelectrode differences. Indeed, further analyses revealed that the patterns of theta-phase coupling are layer-specific (Fig. 5).

Theta Phase Modulates HFOs

Classically, hippocampal high-frequency oscillations in the ripple band (100–250 Hz) occur associated with sharp waves during behavioral immobility, consummatory behaviors, and slow-wave sleep (Buzsaki et al. 1992, 2003; Ylinen et al. 1995; Nguyen et al. 2009). In contrast, hippocampal theta oscillations are most prominent during active waking behavior (e.g., walking, rearing) and REM sleep (Vanderwolf 1969; Timo-Iaria et al. 1970). Based on this difference, it is currently believed that theta oscillations and high-frequency oscillatory activity are mutually exclusive network states associated with entirely different behaviors. Contrary to this classical view, however, our findings show the existence of HFOs concurrent with theta waves. In fact, HFOs not only co-occur but also interact with theta, which suggests that the network mechanisms underlying these rhythms are mechanistically related.

Theta-associated HFO activity has been recently reported in tetrode recordings of rats performing a T-maze task (Tort et al. 2008). In that study, however, the HFOs were only observed by means of CFC analyses, since the PSD exhibited no clear peak in the HFO band. In fact, the absence of HFO activity at the PSD level may explain why these oscillations were not identified before the development of novel CFC tools. In contrast, here we observed a clear PSD peak in the HFO band in superficial electrodes presenting prominent theta-HFO coupling during periods of high theta activity (Fig. 4*B*,*D*). Importantly, the power peak in the 120–160 Hz range does not correspond to the activity of sharp wave–associated ripples, since periods of waking immobility and slow-wave sleep were discarded from this analysis. In fact, despite having overlapping frequency ranges, ripple oscillations and HFOs occur in different CA1 layers and are associated with different behavioral and network states. We further highlight key differences between HFOs and sharp wave–associated ripples in Table 1 and Figure 7.

Recently, sharp wave–associated ripple activity was also described to occur during brief pauses of theta oscillations when rats explore an environment (O'Neill et al. 2006). These oscillations, however, also differ from the HFOs described here in some key aspects; for example, they are characteristically

Downloaded from http://cercor.oxfordjournals.org/ at Brigham & Women's Hospital on November 29, 2012

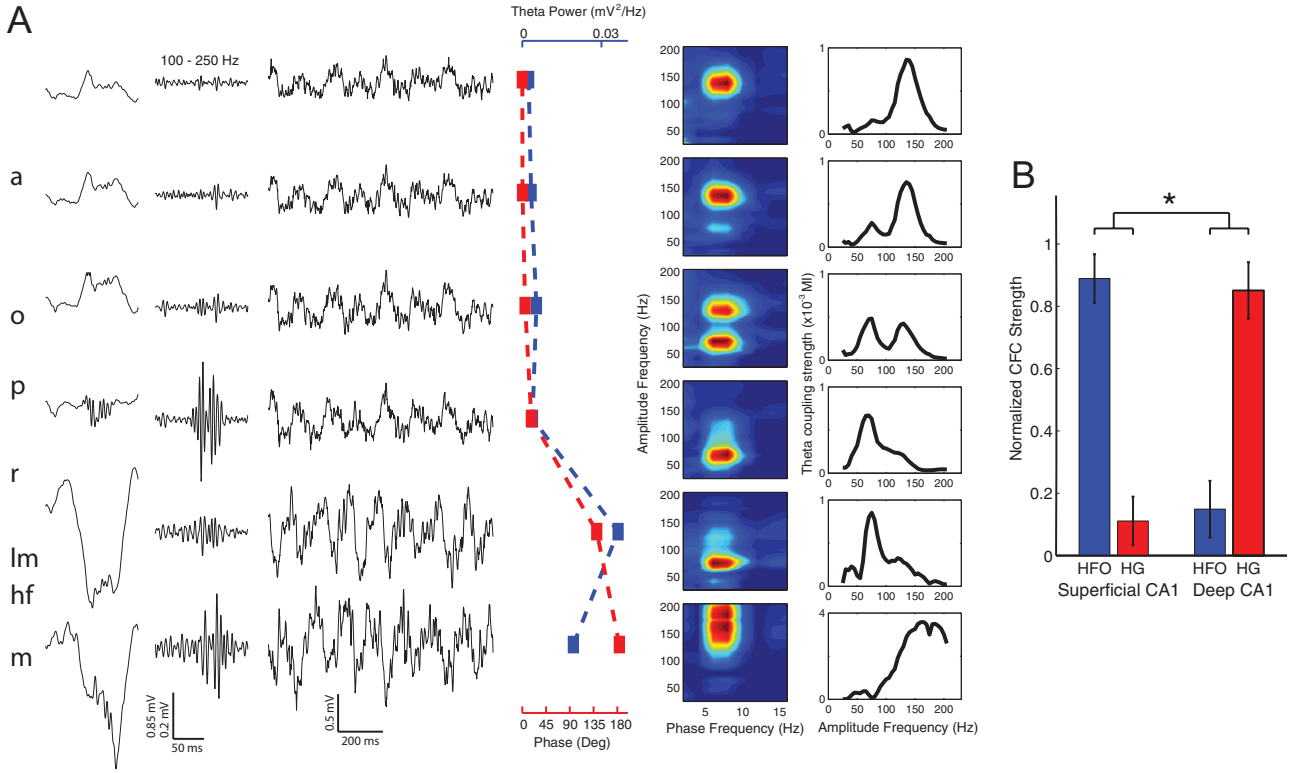

Figure 5. Different CA1 layers have different CFC patterns. (*A*) Comodulation maps and theta coupling strength for 6 electrodes in a bundle (rightmost columns), obtained from the analysis of 300 s of active exploration. The most superficial electrode is shown on top. The third column from right shows peak theta power in each electrode (blue squares) and theta phase difference with respect to the most superficial electrode (red squares). The 2 leftmost columns show a ripple event (LFPs and 100–250 Hz filtered signal) during awake immobility, and the third column from left depicts 1-s long LFPs during a period of high theta activity. Notice prominent ripple activity at the pyramidal layer and increase in theta power along with theta phase reversal in deep electrodes. a—stratum alveus; o—stratum oriens; p—stratum pyramidale; r—stratum radiatum; lm—stratum lacunosum–moleculare; hf—hippocampal fissure; m—molecular layer. (*B*) Normalized theta-HFO (blue) and theta-HG (red) coupling in the most superficial (left bars) and deep (right bars) CA1 electrodes in a vertical bundle (group result; $n = 6$ rats). For each animal, the normalization was performed within electrodes by dividing the MI of each oscillatory coupling (theta-HG or theta-HFO) by its sum over both couplings (e.g., Normalized theta-HFO MI = (Theta-HFO MI)/(Theta-HG MI + Theta-HFO MI). Bars represent mean ± standard deviation. $^*P < 0.0001$ ($F_{1,20}$=457.54; 2-way analysis of variance interaction of electrode location and modulated frequency).

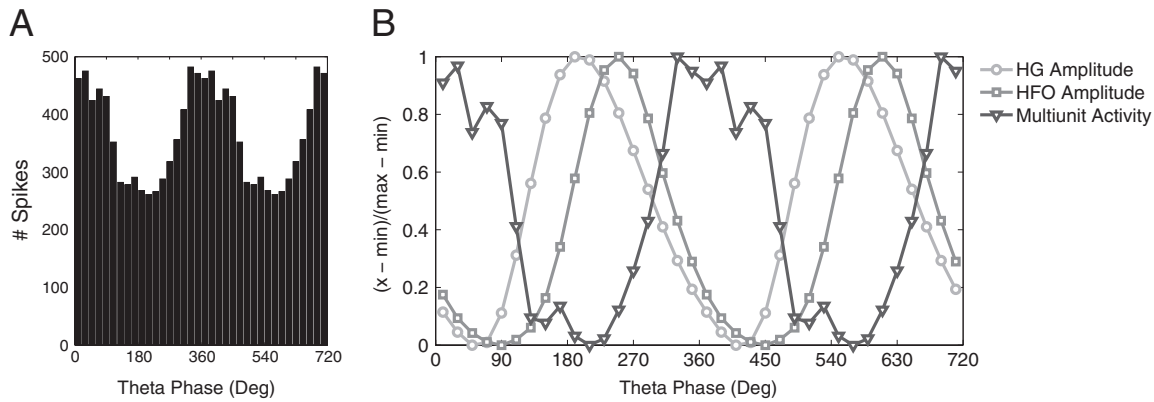

Figure 6. HG, HFO, and multiunit activity are maximal in different theta phases. (*A*) Theta phase histogram for multiunit activity. (*B*) Normalized HG and HFO amplitudes and multiunit activity as a function of the theta phase. The normalization is such that each trace varies from 0 (minimal value) to 1 (maximal value), as indicated in *y*-axis label. The results in *A* and *B* were obtained from pooled data recorded during active waking in 2 rats implanted with electrode bundles. The pyramidal layer theta was used as the reference signal; theta peak corresponds to 180°. HG- and HFO-filtered signals were obtained from electrodes placed in stratum lacunosum–moleculare and stratum oriens–alveus, respectively.

intermittent, that is, by definition, ripples occur as a burst of oscillatory activity which amplitude is higher than a given threshold (usually of several standard deviations above the background mean; Buzsaki et al. 2003; O'Neill et al. 2006). In contrast, HFO activity is continuously present during theta oscillations, has lower amplitude than ripple oscillations, and is not defined by threshold crossing (Fig. 7 and Table 1). Altogether, our CFC and PSD findings demonstrate the existence of theta-associated HFOs that are different from gamma and ripple oscillations.

Downloaded from http://cercor.oxfordjournals.org/ at Brigham & Women's Hospital on November 29, 2012

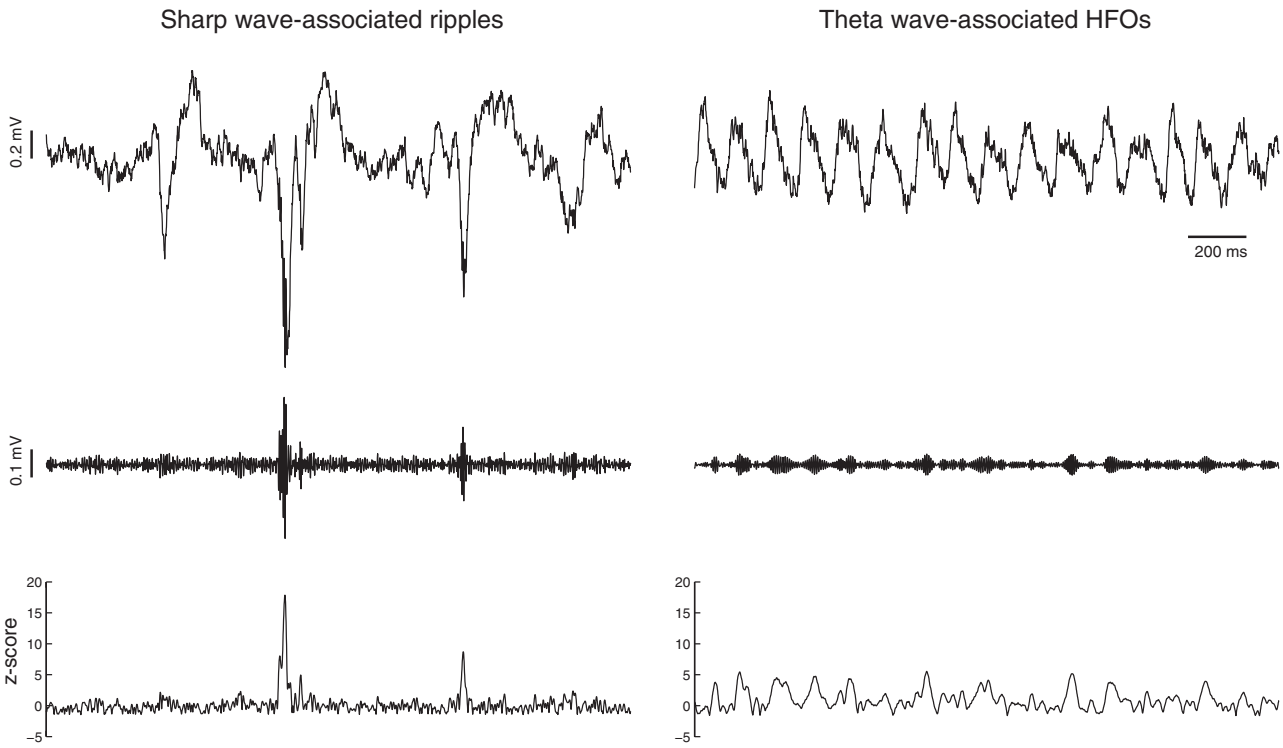

Figure 7. HFOs differ from ripple oscillations. Shown are LFPs (top), filtered signals (middle), and associated amplitude envelopes (bottom) for HFOs (120–160 Hz) (right column) and ripple oscillations (100–250 Hz) (left column). Notice lower amplitude for HFOs compared with ripple events and the continuous presence of theta-modulated HFOs during theta oscillations as opposed to the intermittent nature of sharp wave–associated ripple events.

Table 1
Characteristics differing ripple oscillations and HFOs in CA1

	Ripple oscillations	HFOs
Dynamics	Intermittent	Continuous
Amplitude	High	Low
Cross-frequency interaction	Associated with sharp waves	Associated with theta waves
Behavior	Awake immobility, slow-wave sleep	Active waking, REM sleep
Layer	stratum pyramidale	stratum oriens–alveus

Breaking Gamma into Multiple, Functionally Distinct Oscillations

Our findings and other recent reports (Middleton et al. 2008; Tort et al. 2008, 2010; Colgin et al. 2009; Colgin and Moser 2010) suggest a division of the gamma band (25–150 Hz) into functionally distinct oscillations. The existence of multiple gamma generators in the hippocampal and parahippocampal regions has been proposed before (Bragin et al. 1995; Csicsvari et al. 2003), and differences in their peak frequencies are starting to become clear (Middleton et al. 2008; Tort et al. 2008, 2010; Colgin et al. 2009). For example, it was previously reported that the power of hippocampal LG oscillations decreases while HG power increases during runs in a T-maze task (Tort et al. 2008), suggesting a functional division within the gamma band. Additional evidence comes from the work of Bragin et al. (1995), which showed that HG oscillations in CA1 are replaced by LG after EC lesions. This result suggests that HG depends on EC inputs, while LG depends on CA3. In accordance, Colgin et al. (2009) have recently reported a high degree of coherence between CA3 and CA1 at the slow gamma range and a high degree of coherence between EC and CA1 at the fast gamma range.

Interestingly, while coupling between theta and LG oscillations has been reported intracellularly in both CA1 and CA3 during ketamine–xylazine anesthesia (Soltesz and Deschenes 1993), we did not observe prominent theta-LG coupling in CA1 in our freely behaving animals. It was recently suggested that the EC is the main CA1 gamma source in the absence of CA3 activation (Colgin et al. 2009; Colgin and Moser 2010), consistent with our findings showing a much higher occurrence of theta-HG coupling in CA1. Alternatively, LG may be characteristically less modulated by theta phase in CA1 and would be better observed by other analysis tools such as phase coherence. It is therefore possible that multiplexing of information occurs not only through different frequency channels but also by different types of oscillatory coupling (e.g., phase–phase vs. phase–amplitude). In contrast to the low level of theta-LG coupling in CA1, strong theta-LG coupling has been previously observed in CA3 in freely behaving animals (Tort et al. 2009, 2010), consistent with a role for CA3 in generating LG.

There is not yet a consensus about the exact frequency ranges defining the gamma subbands. Although the higher cutoff frequency employed for classifying low (or slow) gamma seems to be consistent among studies (usually 50 or 60 Hz; Tort et al. 2008; Colgin et al. 2009), the upper frequency bound for high (or fast) gamma has been much more variable. Recent studies in humans and monkeys have used a much broader definition of HG than ours, including frequencies as high as 200 Hz (Edwards et al. 2005; Canolty et al. 2006; Crone et al. 2006; Ray, Crone, et al. 2008; Ray, Niebur, et al. 2008; Jia and Kohn 2011; Ray and Maunsell 2011). However, the present results show that there are at least 2 concurrent but distinct oscillations

Downloaded from http://cercor.oxfordjournals.org/ at Brigham & Women's Hospital on November 29, 2012

within this frequency range in the rat hippocampus. Likewise, Colgin et al. (2009) defined their fast gamma range as 60–140 Hz; such frequency range encompasses our definition of HG as well considerably overlaps with our definition of HFOs.

In summary, mounting evidence indicates that gamma oscillations comprise multiple, distinct fast rhythmic activities. Along with previous work (Tort et al. 2009, 2010), the present results point to at least 3 functionally distinct subbands of fast oscillatory activity concurrent with theta waves in the hippocampus: LG, HG, and HFOs.

Multiple CFC Patterns Across CA1 Layers

The fact that HFOs and HG occur in different theta phases and couple to theta in different CA1 layers strongly suggests that HG and HFOs are distinct physiological processes subserving different functions. Given the deeper location of theta-HG coupling, a main possibility is that HG results from the direct projection of layer III of EC to CA1 stratum lacunosum–moleculare (Steward and Scoville 1976). This deduction based on CFC analysis is in full agreement with previous interregional (EC–CA1) coherence analysis (Colgin et al. 2009) and EC lesion studies (Bragin et al. 1995). HG could be therefore a frequency range used for transmitting spatial/context information from EC to CA1. Gamma oscillations have been previously proposed to generate temporal windows for effective neuronal communication (Fries 2005). Interestingly, the temporal windows of HG (~12.5 ms) might be optimal for spike timing–dependent plasticity to occur (Markram et al. 1997). Moreover, most long-term potentiation induction protocols use 100 Hz bursts of 7 stimulations with an interburst interval of 3–5 Hz (Larson et al. 1986), which roughly corresponds to HG activity nested in a theta rhythm. It is also possible that HG oscillations result from feed-forward inhibition of perforant path projections to CA1 (Buzsaki et al. 1995; Empson and Heinemann 1995), in which case HG would help selecting which neurons undergo synaptic plasticity (Levy et al. 1998). Overall, these observations suggest that HG could have a role in memory encoding (see also Colgin and Moser 2010).

Theta-HFO coupling, in turn, was most apparent above the stratum pyramidale, at the stratum oriens–alveus level. One possibility is that HFOs result from local activity of principal cells. This would be consistent with prominent theta-HFO coupling at superficial CA1 layers, closer to the axons of pyramidal cells, and with recent reports showing a very close relationship between the time course of power variations of high-frequency LFP oscillations (including the HFO band) and the spike frequency of neurons (Ray, Crone, et al. 2008; Khawaja et al. 2009; Jia and Kohn 2011; Ray and Maunsell 2011). Moreover, the phase lag between HG and HFO maximal amplitude within the theta cycle (Fig. 3) is compatible with feed-forward synaptic transmission; therefore, HG and HFOs could be related to CA1 input and output activities, respectively. However, as extensively documented in previous studies (Buzsaki et al. 1983; Fox et al. 1986; Csicsvari et al. 1999; Klausberger et al. 2003; Mizuseki et al. 2011) and replicated in Figure 6, pyramidal cells are most active near the trough of the theta cycle recorded at the pyramidal layer, which is not the same theta phase of peak HFO amplitude. We therefore believe that it is unlikely that HFOs are straightforwardly related to somatic spikes; it may be that "spectral leakage" of the spike shape into a broad band of high-frequency oscillations is only noticeable in the absence of genuine fast oscillations (see also Colgin et al. 2009; Jackson et al. 2011).

In the hippocampus, inhibitory interneurons contribute to producing fast field oscillations such as sharp wave–associated ripples (Ylinen et al. 1995). It is therefore possible that field HFOs also depend on inhibitory postsynaptic potentials. In accordance to this, a recent in vitro work has shown hippocampal HFOs modulated by theta (termed "fast gamma" in this work), which were sensitive to bicuculline but not DNQX (Jackson et al. 2011). A possible role for inhibitory interneurons in contributing to field HFOs is also consistent with the fact that some interneuron subtypes spike some degrees after the peak of theta oscillations (Klausberger et al. 2003; Klausberger and Somogyi 2008), near where HFO amplitude is maximal.

It should be noted, however, that oscillations of similar frequency as the theta-associated HFOs can be observed when synaptic transmission is blocked (Draguhn et al. 1998; Nimmrich et al. 2005). In fact, Traub and colleagues have been describing very fast oscillations (VFOs) generated in the stratum oriens–alveus and putatively attributed to axonal gap junctions (Draguhn et al. 1998; Traub et al. 2002, 2003). For instance, they showed that high-frequency field activity (~148 Hz) can be induced by kainate in an in vitro preparation where the stratum oriens–alveus was surgically isolated from the pyramidal layer (Traub et al. 2003). Moreover, this high-frequency activity coexisted with and was modulated by gamma oscillations (Traub et al. 2003). Whether the theta-associated HFOs we observed in vivo are the same as the VFOs dependent on axonal gap junctions reported in vitro by Traub and colleagues is yet to be determined. Knowing the cellular and network mechanisms underlying the generation of theta-associated HFOs should help understanding their function, if any.

Limitations

To date, there is no measure that is able to assess the instantaneous levels of phase–amplitude coupling, that is, all phase–amplitude coupling measures have a time-resolution limitation (Tort et al. 2010). In order to assess CFC, one needs to analyze a time series long enough such that enough oscillatory cycles of the phase-modulating frequency are sampled to allow capturing true coupling effects while averaging out noise (Tort et al. 2010). In this work, using a time resolution of 60 s, we showed that theta-HG and theta-HFO coupling occur as long as the field potentials also exhibit theta oscillations (Fig. 2*A*). We obtained similar results when using shorter time windows (Supplementary Fig. S3), but it remains to be established whether or not theta-phase coupling always accompany theta oscillations on a finer temporal scale. Another point of future investigation is to understand why some oscillatory activities are observable mainly under CFC analysis but not under Fourier analysis: for instance, while we found that HG was clearly modulated by theta phase, the PSD showed little evidence of a sustained rhythm at this frequency range (Figs 2*B* and 4*D*; if anything, Fig. 4*D* shows presence of broad band gamma activity, including LG and HG). We note that the existence of coupling in the absence of a power peak has also been observed in previous work (Tort et al. 2008; Axmacher et al. 2010; Jackson et al. 2011), while many other CFC studies did not report the PSD values up to the amplitude-modulated band.

Downloaded from http://cercor.oxfordjournals.org/ at Brigham & Women's Hospital on November 29, 2012

Conclusion

In all, our CFC findings are in accordance with the recent proposal of different gamma subbands routing the information flow into CA1 and in particular with the suggestion that the communication between EC and CA1 occurs through HG oscillations (Colgin et al. 2009). In addition, our work reveals a novel type of fast oscillatory activity in CA1 different from fast gamma oscillations and demonstrates a topological dependence of HG and HFOs on CA1 layer.

Supplementary Material

Supplementary material can be found at: http://www.cercor.oxfordjournals.org/

Funding

Conselho Nacional de Desenvolvimento Científico e Tecnológico, Coordenação de Aperfeiçoamento de Pessoal de Nível Superior, Fundação de Apoio à Pesquisa do Estado do Rio Grande do Norte, Pew Latin American Fellows Program in the Biomedical Sciences, and Associação Alberto Santos Dumont para Apoio à Pesquisa.

Notes

We thank Richardson Leão and Jurij Brankačk for helpful comments on an earlier version of the manuscript, Joanilson Guimarães for help with histology, and Claudio Queiroz, Rodrigo Romcy-Pereira, and Kelly Soares for help with evoked responses and electrode bundle placement. *Conflict of Interest* : None declared.

References

Axmacher N, Henseler MM, Jensen O, Weinreich I, Elger CE, Fell J. 2010. Cross-frequency coupling supports multi-item working memory in the human hippocampus. Proc Natl Acad Sci U S A. 107:3228–3233.

Bragin A, Jando G, Nadasdy Z, Hetke J, Wise K, Buzsaki G. 1995. Gamma (40-100 Hz) oscillation in the hippocampus of the behaving rat. J Neurosci. 15:47–60.

Brankack J, Stewart M, Fox SE. 1993. Current source density analysis of the hippocampal theta rhythm: associated sustained potentials and candidate synaptic generators. Brain Res. 615:310–327.

Buzsaki G, Buhl DL, Harris KD, Csicsvari J, Czeh B, Morozov A. 2003. Hippocampal network patterns of activity in the mouse. J Neurosci. 116:201–211.

Buzsaki G, Horvath Z, Urioste R, Hetke J, Wise K. 1992. High-frequency network oscillation in the hippocampus. Science. 256:1025–1027.

Buzsaki G, Leung LW, Vanderwolf CH. 1983. Cellular bases of hippocampal EEG in the behaving rat. Brain Res. 287:139–171.

Buzsaki G, Penttonen M, Bragin A, Nadasdy Z, Chrobak JJ. 1995. Possible physiological role of the perforant path-CA1 projection. Hippocampus. 5:141–146.

Canolty RT, Edwards E, Dalal SS, Soltani M, Nagarajan SS, Kirsch HE, Berger MS, Barbaro NM, Knight RT. 2006. High gamma power is phase-locked to theta oscillations in human neocortex. Science. 313:1626–1628.

Canolty RT, Knight RT. 2010. The functional role of cross-frequency coupling. Trends Cogn Sci. 14:506–515.

Cohen MX, Axmacher N, Lenartz D, Elger CE, Sturm V, Schlaepfer TE. 2009. Good vibrations: cross-frequency coupling in the human nucleus accumbens during reward processing. J Cogn Neurosci. 21:875–889.

Colgin LL, Denninger T, Fyhn M, Hafting T, Bonnevie T, Jensen O, Moser MB, Moser EI. 2009. Frequency of gamma oscillations routes flow of information in the hippocampus. Nature. 462:353–357.

Colgin LL, Moser EI. 2010. Gamma oscillations in the hippocampus. Physiol (Bethesda). 25:319–329.

Crone NE, Sinai A, Korzeniewska A. 2006. High-frequency gamma oscillations and human brain mapping with electrocorticography. Prog Brain Res. 159:275–295.

Csicsvari J, Hirase H, Czurko A, Mamiya A, Buzsaki G. 1999. Oscillatory coupling of hippocampal pyramidal cells and interneurons in the behaving rat. J Neurosci. 19:274–287.

Csicsvari J, Jamieson B, Wise KD, Buzsaki G. 2003. Mechanisms of gamma oscillations in the hippocampus of the behaving rat. Neuron. 37:311–322.

Delorme A, Makeig S. 2004. EEGLAB: an open source toolbox for analysis of single-trial EEG dynamics including independent component analysis. J Neurosci Methods. 134:9–21.

Draguhn A, Traub RD, Schmitz D, Jefferys JGR. 1998. Electrical coupling underlies high-frequency oscillations in the hippocampus in vitro. Nature. 394:189–192.

Dzirasa K, Ribeiro S, Costa R, Santos LM, Lin SC, Grosmark A, Sotnikova TD, Gainetdinov RR, Caron MG, Nicolelis MA. 2006. Dopaminergic control of sleep-wake states. J Neurosci. 26:10577–10589.

Edwards E, Soltani M, Deouell LY, Berger MS, Knight RT. 2005. High gamma activity in response to deviant auditory stimuli recorded directly from human cortex. J Neurophysiol. 94:4269–4280.

Empson RM, Heinemann U. 1995. The perforant path projection to hippocampal area CA1 in the rat hippocampal-entorhinal cortex combined slice. J Physiol. 484(Pt 3):707–720.

Fox SE, Wolfson S, Ranck JB Jr. 1986. Hippocampal theta rhythm and the firing of neurons in walking and urethane anesthetized rats. Exp Brain Res. 62:495–508.

Fries P. 2005. A mechanism for cognitive dynamics: neuronal communication through neuronal coherence. Trends Cogn Sci. 9:474–480.

Gervasoni D, Lin SC, Ribeiro S, Soares ES, Pantoja J, Nicolelis MA. 2004. Global forebrain dynamics predict rat behavioral states and their transitions. J Neurosci. 24:11137–11147.

Jackson J, Goutagny R, Williams S. 2011. Fast and slow gamma rhythms are intrinsically and independently generated in the subiculum. J Neurosci. 31:12104–12117.

Jensen O, Colgin LL. 2007. Cross-frequency coupling between neuronal oscillations. Trends Cogn Sci. 11:267–269.

Jia X, Kohn A. 2011. Gamma rhythms in the brain. PLoS Biol. 9:e1001045.

Kendrick KM, Zhan Y, Fisher H, Nicol AU, Zhang X, Feng J. 2011. Learning alters theta amplitude, theta-gamma coupling and neuronal synchronization in inferotemporal cortex. BMC Neurosci. 12:55.

Khawaja FA, Tsui JM, Pack CC. 2009. Pattern motion selectivity of spiking outputs and local field potentials in macaque visual cortex. J Neurosci. 29:13702–13709.

Klausberger T, Magill PJ, Marton LF, Roberts JD, Cobden PM, Buzsaki G, Somogyi P. 2003. Brain-state- and cell-type-specific firing of hippocampal interneurons in vivo. Nature. 421:844–848.

Klausberger T, Somogyi P. 2008. Neuronal diversity and temporal dynamics: the unity of hippocampal circuit operations. Science. 321:53–57.

Kramer MA, Tort AB, Kopell NJ. 2008. Sharp edge artifacts and spurious coupling in EEG frequency comodulation measures. J Neurosci Methods. 170:352–357.

Lakatos P, Shah AS, Knuth KH, Ulbert I, Karmos G, Schroeder CE. 2005. An oscillatory hierarchy controlling neuronal excitability and stimulus processing in the auditory cortex. J Neurophysiol. 94:1904–1911.

Larson J, Wong D, Lynch G. 1986. Patterned stimulation at the theta frequency is optimal for the induction of hippocampal long-term potentiation. Brain Res. 368:347–350.

Levy WB, Desmond NL, Zhang DX. 1998. Perforant path activation modulates the induction of long-term potentiation of the schaffer collateral–hippocampal CA1 response: theoretical and experimental analyses. Learn Mem. 4:510–518.

Lisman JE, Idiart MA. 1995. Storage of 7 +/- 2 short-term memories in oscillatory subcycles. Science. 267:1512–1515.

Lubenov EV, Siapas AG. 2009. Hippocampal theta oscillations are travelling waves. Nature. 459:534–539.

Downloaded from http://cercor.oxfordjournals.org/ at Brigham & Women's Hospital on November 29, 2012

Markram H, Lubke J, Frotscher M, Sakmann B. 1997. Regulation of synaptic efficacy by coincidence of postsynaptic APs and EPSPs. Science. 275:213–215.
Middleton S, Jalics J, Kispersky T, Lebeau FE, Roopun AK, Kopell NJ, Whittington MA, Cunningham MO. 2008. NMDA receptor-dependent switching between different gamma rhythm-generating microcircuits in entorhinal cortex. Proc Natl Acad Sci U S A. 105:18572–18577.
Miller KJ, Hermes D, Honey CJ, Sharma M, Rao RP, den Nijs M, Fetz EE, Sejnowski TJ, Hebb AO, Ojemann JG, et al. 2010. Dynamic modulation of local population activity by rhythm phase in human occipital cortex during a visual search task. Front Hum Neurosci. 4:197.
Mizuseki K, Diba K, Pastalkova E, Buzsaki G. 2011. Hippocampal CA1 pyramidal cells form functionally distinct sublayers. Nat Neurosci. 14:1174–1181.
Nguyen DP, Kloosterman F, Barbieri R, Brown EN, Wilson MA. 2009. Characterizing the dynamic frequency structure of fast oscillations in the rodent hippocampus. Front Integr Neurosci. 3:11.
Nimmrich V, Maier N, Schmitz D, Draguhn A. 2005. Induced sharp wave-ripple complexes in the absence of synaptic inhibition in mouse hippocampal slices. J Physiol. 563:663–670.
O'Neill J, Senior T, Csicsvari J. 2006. Place-selective firing of CA1 pyramidal cells during sharp wave/ripple network patterns in exploratory behavior. Neuron. 49:143–155.
Onslow AC, Bogacz R, Jones MW. 2011. Quantifying phase-amplitude coupling in neuronal network oscillations. Prog Biophys Mol Biol. 105:49–57.
Ray S, Crone NE, Niebur E, Franaszczuk PJ, Hsiao SS. 2008. Neural correlates of high-gamma oscillations (60-200 Hz) in macaque local field potentials and their potential implications in electrocorticography. J Neurosci. 28:11526–11536.
Ray S, Maunsell JH. 2011. Different origins of gamma rhythm and high-gamma activity in macaque visual cortex. PLoS Biol. 9:e1000610.
Ray S, Niebur E, Hsiao SS, Sinai A, Crone NE. 2008. High-frequency gamma activity (80-150Hz) is increased in human cortex during selective attention. Clin Neurophysiol. 119:116–133.
Ribeiro S, Shi X, Engelhard M, Zhou Y, Zhang H, Gervasoni D, Lin SC, Wada K, Lemos NA, Nicolelis MA. 2007. Novel experience induces persistent sleep-dependent plasticity in the cortex but not in the hippocampus. Front Neurosci. 1:43–55.
Schroeder CE, Lakatos P. 2009. Low-frequency neuronal oscillations as instruments of sensory selection. Trends Neurosci. 32:9–18.
Soltesz I, Deschenes M. 1993. Low- and high-frequency membrane potential oscillations during theta activity in CA1 and CA3 pyramidal neurons of the rat hippocampus under ketamine-xylazine anesthesia. J Neurophysiol. 70:97–116.
Steward O, Scoville SA. 1976. Cells of origin of entorhinal cortical afferents to the hippocampus and fascia dentata of the rat. J Comp Neurol. 169:347–370.
Stumpf C. 1965. The fast component in the electrical activity of rabbit's hippocampus. Electroencephalogr Clin Neurophysiol. 18:477–486.
Timo-Iaria C, Negrao N, Schmidek WR, Hoshino K, Lobato de Menezes CE, Leme da Rocha T. 1970. Phases and states of sleep in the rat. Physiol Behav. 5:1057–1062.
Tort AB, Komorowski R, Eichenbaum H, Kopell N. 2010. Measuring phase-amplitude coupling between neuronal oscillations of different frequencies. J Neurophysiol. 104:1195–1210.
Tort AB, Komorowski RW, Manns JR, Kopell NJ, Eichenbaum H. 2009. Theta-gamma coupling increases during the learning of item-context associations. Proc Natl Acad Sci U S A. 106:20942–20947.
Tort AB, Kramer MA, Thorn C, Gibson DJ, Kubota Y, Graybiel AM, Kopell NJ. 2008. Dynamic cross-frequency couplings of local field potential oscillations in rat striatum and hippocampus during performance of a T-maze task. Proc Natl Acad Sci U S A. 105:20517–20522.
Traub RD, Cunningham MO, Gloveli T, LeBeau FE, Bibbig A, Buhl EH, Whittington MA. 2003. GABA-enhanced collective behavior in neuronal axons underlies persistent gamma-frequency oscillations. Proc Natl Acad Sci U S A. 100:11047–11052.
Traub RD, Draguhn A, Whittington MA, Baldeweg T, Bibbig A, Buhl EH, Schmitz D. 2002. Axonal gap junctions between principal neurons: a novel source of network oscillations, and perhaps epileptogenesis. Rev Neurosci. 13:1–30.
Vanderwolf CH. 1969. Hippocampal electrical activity and voluntary movement in the rat. Electroencephalogr Clin Neurophysiol. 26:407–418.
Vanhatalo S, Palva JM, Holmes MD, Miller JW, Voipio J, Kaila K. 2004. Infraslow oscillations modulate excitability and interictal epileptic activity in the human cortex during sleep. Proc Natl Acad Sci U S A. 101:5053–5057.
Voytek B, Canolty RT, Shestyuk A, Crone NE, Parvizi J, Knight RT. 2010. Shifts in gamma phase-amplitude coupling frequency from theta to alpha over posterior cortex during visual tasks. Front Hum Neurosci. 4:191.
Whittingstall K, Logothetis NK. 2009. Frequency-band coupling in surface EEG reflects spiking activity in monkey visual cortex. Neuron. 64:281–289.
Wulff P, Ponomarenko AA, Bartos M, Korotkova TM, Fuchs EC, Bahner F, Both M, Tort AB, Kopell NJ, Wisden W, et al. 2009. Hippocampal theta rhythm and its coupling with gamma oscillations require fast inhibition onto parvalbumin-positive interneurons. Proc Natl Acad Sci U S A. 106:3561–3566.
Ylinen A, Bragin A, Nadasdy Z, Jando G, Szabo I, Sik A, Buzsaki G. 1995. Sharp wave-associated high-frequency oscillation (200 Hz) in the intact hippocampus: network and intracellular mechanisms. J Neurosci. 15:30–46.

Downloaded from http://cercor.oxfordjournals.org/ at Brigham & Women's Hospital on November 29, 2012